Aromatase Inhibitors: Synthesis, Biological Activity, and Binding Mode of Azole-Type Compounds

P. Furet,* C. Batzl, A. Bhatnagar, E. Francotte, G. Rihs, and M. Lang

Research Department, Pharmaceuticals Division, CIBA-GEIGY Ltd., CH-4002 Basle, Switzerland

Received September 23, 1992

The enantiomers of the potent nonsteroidal inhibitor of aromatase fadrozole hydrochloride 3 have been separated and their absolute configuration determined by X-ray crystallography. On the basis of a molecular modeling comparison of the active enantiomer 4 and one of the most potent steroidal inhibitors reported to date, (19*R*)-10-thiiranylestr-4-ene-3,17-dione, 7, a model describing the relative binding modes of the azole-type and steroidal inhibitors of aromatase at the active site of the enzyme is proposed. It is suggested that the cyanophenyl moiety present in the most active azole inhibitors partially mimics the steroid backbone of the natural substrate for aromatase, androst-4-ene-3,17-dione, 1. The synthesis and biological testing of novel analogues of 3 used to define the accessible and nonaccessible volumes to ligands in the model of the active site of aromatase are reported.

Introduction

Aromatase is the cytochrome P-450 dependent enzyme which catalyses the final step in the biosynthesis of estrogens. Inhibition of this enzyme as a mechanism for inhibiting estrogen biosynthesis has been the goal of the efforts of many research groups worldwide because it has been identified as a good therapeutic strategy for the treatment of estrogen-dependent breast cancers.[1-3] These efforts have resulted in the identification of structurally diverse, potent inhibitors of aromatase that can be grouped in the following three classes: (1) steroidal analogues of androst-4-ene-3,17-dione (AD, 1), the natural substrate of aromatase; (2) analogues of aminoglutethimide (AG, 2), the only nonsteroidal inhibitor of aromatase introduced in the market so far; and (3) heterocyclic azole compounds exemplified by CGS 16949A (fadrozole hydrochloride,[4] 3), a potent nonsteroidal inhibitor currently in clinical evaluation.

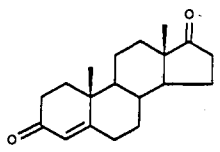

1; AD

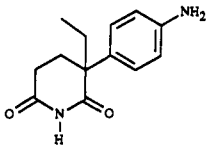

2; AG

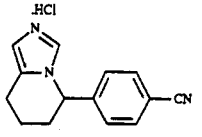

3; CGS 16949A

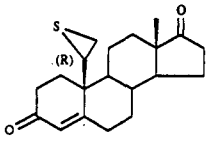

7; 10-Thiiranyl-AD

To aid us in our research for new inhibitors of aromatase which were more potent and selective than AG, we initiated molecular modeling studies aimed at the mapping of the active site of the enzyme. In the absence of any direct information on the tertiary structure of aromatase, our modeling efforts rely on the conformational analysis of the chemical structures of known aromatase inhibitors. Thus, we report structural comparisons between azole-type and the most potent steroidal inhibitors described in the literature which have led to a model describing the relative binding modes of these two classes of inhibitors at the active site of the enzyme. The synthesis and biological testing of some novel analogues of 3 used in the definition and validation of the model are described.

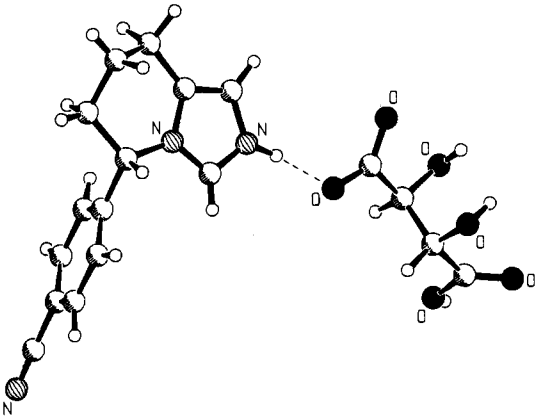

Figure 1. X-ray structure of the salt from 4 and D-(−)-tartaric acid.

Chemistry and Biological Properties

The enantiomers (−)-4 and (+)-5 of fadrozole hydrochloride[4] (3) were separated by HPLC on benzoylcellulose beads.[5] The (−)-enantiomer 4 was assigned the absolute *S* configuration after X-ray analysis of its corresponding salt with D-(−)-tartaric acid (Figure 1). The highly active 4-(methylene-1-imidazolylmethyl)benzonitrile (6) was prepared from 4-(1-imidazolylmethyl)benzonitrile and paraformaldehyde according to a procedure described in the literature,[6] and the bicyclic analogue 8 was obtained from the reaction of 6-cyano-1-tetralon[7] with imidazole and thionyl chloride. The formal structural hybride of 3 and 9, 5,5-bis(4-cyanophenyl)-5,6,7,8-tetrahydroimidazo[1,5-*a*]pyridine, 10, was synthesized[6] through arylation of the anion of fadrozole hydrochloride 3 with 4-fluorobenzonitrile. Using a published procedure,[8] the treatment of the imidoyl chloride, obtained from *N*-(4-bromophenyl)-4-cyanobenzamide and thionyl chloride, with imidazole provided the imine derivative 11. With the exception of

0022-2623/93/1836-1393$04.00/0

Table I. In Vitro Inhibition of Human Placental Aromatase

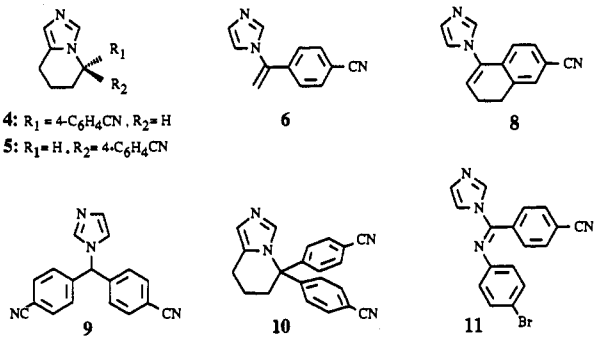

compd	IC_{50}[a] (nM)	relative potency[b]
4	3.2	590
5	680	3
6	0.7	2700
8	2.9	660
9	3.5	540
10	233	8
11	7.7	250

[a] Inhibitor concentration required to inhibit enzyme activity by 50%. [b] Calculated from the IC_{50} values and relative to AG (IC_{50} = 1900 nM).

Table II. Equilibrium Conformations of 4

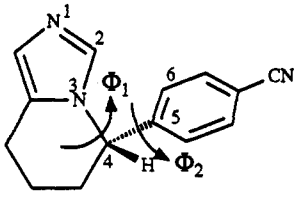

Φ_1: C(2)N(3)-C(4)C(5)

Φ_2: N(3)C(4)-C(5)C(6)

compd	Φ_1[a]	Φ_2[a]	ΔE[b]
4A	-36	120	0.0
4B	-72	140	2.0

[a] Torsional angles in degrees. [b] Relative energies in kcal/mol.

the *R* enantiomer of fadrozole hydrochloride **5** and the bulky derivative **10** all investigated azole-type compounds were found to be highly potent inhibitors of aromatase (Table I).

Molecular Modeling

Active Conformation of 3. The separation of **3** into its enantiomers (−)-**4** and (+)-**5** demonstrated that the (−)-enantiomer with the *S* absolute configuration was responsible for the high aromatase inhibitory activity of **3**. The conformational analysis of **4** reveals that the molecule can adopt two equilibrium conformations, **4A** and **4B** (Table II), which are separated by an energy gap of approximately 2 kcal/mol and correspond respectively to a quasi-equatorial and a quasi-axial orientation of the cyanophenyl ring. To determine which conformation **4** adopts when it binds to the active site of aromatase, we considered compound **6**, a potent analogue (Table I) in which a vinyl function has been introduced between the imidazole and cyanophenyl moieties. The conformational analysis of this compound revealed that it possesses only one conformation in common with **4** in terms of the spatial disposition of the imidazole and cyanophenyl moieties. This conformation corresponds to values of the torsion angles Φ_1 and Φ_2 approximating those of the equatorial conformation **4A**, which led us to conclude that the latter conformation which is also observed in the crystal structure reported in Figure 1 is likely to be the active conformation of **4** for aromatase inhibition. Consequently, it was used to represent fadrozole hydrochloride (**3**) in the subsequent modeling studies.

Comparison of 4 and 10-Thiiranyl-AD, 7. The basis of a binding model for both azole-type inhibitors and steroidal inhibitors at the active site of aromatase can be defined by comparing **4** to (19*R*)-10-thiiranylestr-4-ene-3,17-dione (10-thiiranyl-AD, **7**), a potent reversible inhibitor (K_i = 2 nM).[9] Both inhibitors coordinate to the iron atom of the heme group present at the active site of the enzyme as shown by a type II cytochrome P-450 binding spectrum.[4,9] The observation of a type II spectrum provides information concerning the spatial disposition of the heme-binding moieties of these inhibitors, the imidazole and thiirane rings, at the active site of aromatase since the geometries of coordination of these types of ligands to a porphyrin nucleus have been well characterized by experimental and theoretical studies.[10-13] This is illustrated in Figure 2 by a model of an imidazole and a thiirane ring coordinating to a porphyrin nucleus constructed by using the X-ray structures of porphyrin complexes involving similar ligands, retrieved from the Cambridge database.[14a,b] This anchorage point in the cavity of aromatase being well defined for both inhibitors, additional similarities between their 3-D structures were sought.

Since a cyano function in the para position of the phenyl ring is an essential structural requirement for high inhibitory activity in **3** and its analogues,[4,15] it would seem possible that this polar group might mimic one of the carbonyl functions of the steroidal inhibitor, either that of the A or that of the D ring. Thus for each case, the calculated minimum-energy conformations of **7** were superimposed on the active conformation of **4** determined as described previously. The positions of the cyano and carbonyl functions were matched while maintaining the most probable geometries of coordination of the imidazole and thiirane moieties shown in Figure 2 (the most probable geometry would be a sp^2 geometry of coordination with a nitrogen–iron distance of approximately 2.0 Å for the imidazole ligand and a sp^3 geometry with a sulfur–iron distance of approximately 2.3 Å for the thioether ligand). This procedure did not lead to any reasonable fit when the carbonyl function of the A ring was used. In contrast, with the carbonyl of ring D it was possible to obtain an excellent superposition in which the steroid molecule adopts its calculated lowest energy conformation. This superposition, shown in Figure 3, constitutes the basis of our model for the relative binding modes of the imidazole and steroidal inhibitors of aromatase. As can be seen in Figure 3, not only the polar groups but also hydrophobic parts of the molecules overlap; in particular the phenyl ring of **4** superimposes very well with the C ring of the steroid, and the saturated piperidine ring of **4** has some molecular volume in common with the A ring. The essence of our model lies therefore in the hypothesis that the cyanophenyl moiety of **4** and its analogues is able to mimic some essential structural features of the steroid skeleton of the substrate analogues. In this context the high activity of the imidazole inhibitor may be considered to be the result of the synergistic use of two properties

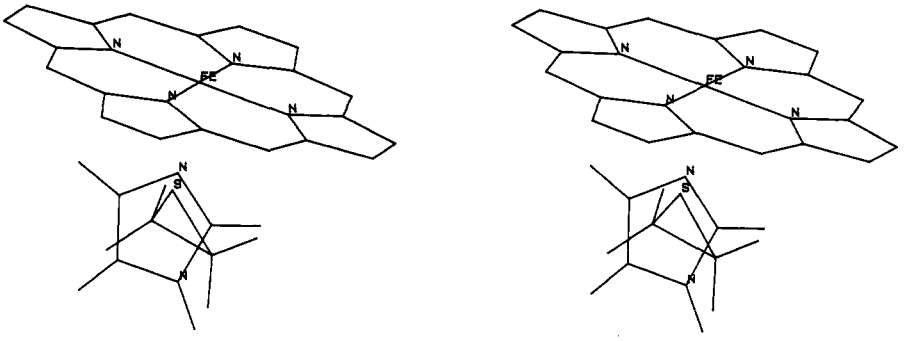

Figure 2. Model representing an imidazole and a thiirane ring complexing a porphyrin nucleus (stereoscopic view). The geometries of coordination were constructed by using the X-ray structures of the following complexes retrieved from the Cambridge database:[14a] (i) imidazole ligand: bis(imidazole)(meso-tetraphenylporphinato)iron(III) chloride,[14b] entry code FEJDED; (ii) thiirane ligand: bis-(pentamethylene sulfide)(meso-tetraphenylporphinato)iron(III) perchlorate,[11] entry code TPPSFE10.

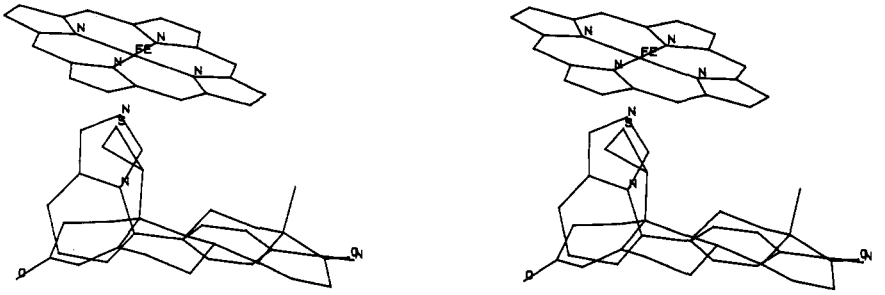

Figure 3. Superposition of 4 and 10-thiiranyl-AD (7) defining our model for the relative binding modes of the imidazole and steroid inhibitors of aromatase (stereoscopic view).

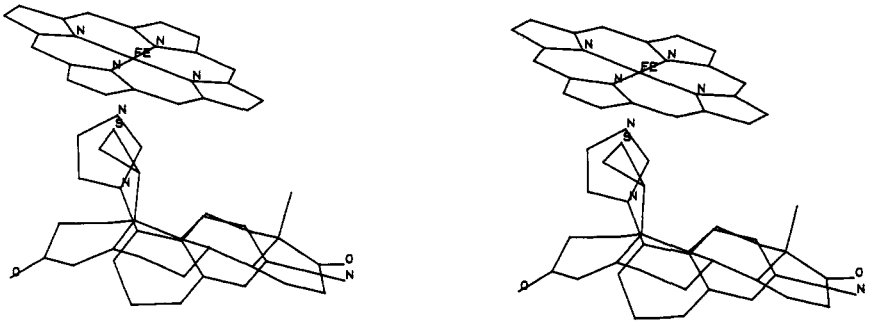

Figure 4. Superposition of designed structure 8 and 10-thiiranyl-AD (7) (stereoscopic view).

leading to strong binding interactions with the enzyme: the heme coordination property of the imidazole ring and the ability of the other portion of the molecule to exploit some of the interactions used by the enzyme to bind the steroid skeleton of its natural substrate, assuming that the binding mode of 10-thiiranyl-AD (7) is representative of that of AD.[9] Besides the geometric aspects discussed above, there is additional evidence in support of this model. Recent structure–activity studies with 3-deoxy analogues of AD by Numazawa et al.[16,17] have demonstrated the importance of the carbonyl function of the D ring for tight binding to aromatase while it has been observed that the presence of this functional group on ring A is not essential for activity. In addition, Sherwin et al.[18] have estimated, on the basis of a study of AD analogues, that the carbonyl group of the D ring contributes a significant 1 kcal/mol to the free energy of binding of AD (1). These studies, in conjunction with the modeling analysis reported here, do not support an early model proposed by Banting et al.[19] in which it is claimed that the cyano group of fadrozole hydrochloride (3) may act as a mimic of the carbonyl function of the A ring of AD (1). To further test our model, 4, the active enantiomer of 3, was replaced by much weaker analogues in which the cyano function has been shifted to the meta or ortho position of the phenyl ring.[4,15] No really satisfactory superpositions with the steroidal inhibitor could be obtained. Figure 3 shows that in our model 4 does not possess any structural element occupying the region of space corresponding to the B ring of the steroid molecule. To even further test the validity of our model, compound 8 was synthesized. In this analogue of 4, a cyclization was designed in such a way that the new ring formed could mimic the B ring of the steroid as shown in Figure 4. In full agreement with the modeling considerations, 8 exhibits a high level of activity comparable to that of 4 (Table I).

Positioning of CGS 18320B (9) in the Model. CGS 18320B, 9, is a potent[20] noncyclized analogue of fadrozole hydrochloride bearing a second cyanophenyl group at the central carbon atom of the molecule. This additional bulky moiety, well accepted by the enzyme, was of interest in the mapping of its active site. A modeling study was therefore undertaken to position 9 in our proposed model. Comparison of the calculated low-energy conformations of 9 with the presumed active conformations of 4 in terms of overlap of the (cyanobenzyl)imidazole moieties showed that there are two possible ways, labeled A and B in Figure 5, to superimpose the two molecules. We could determine

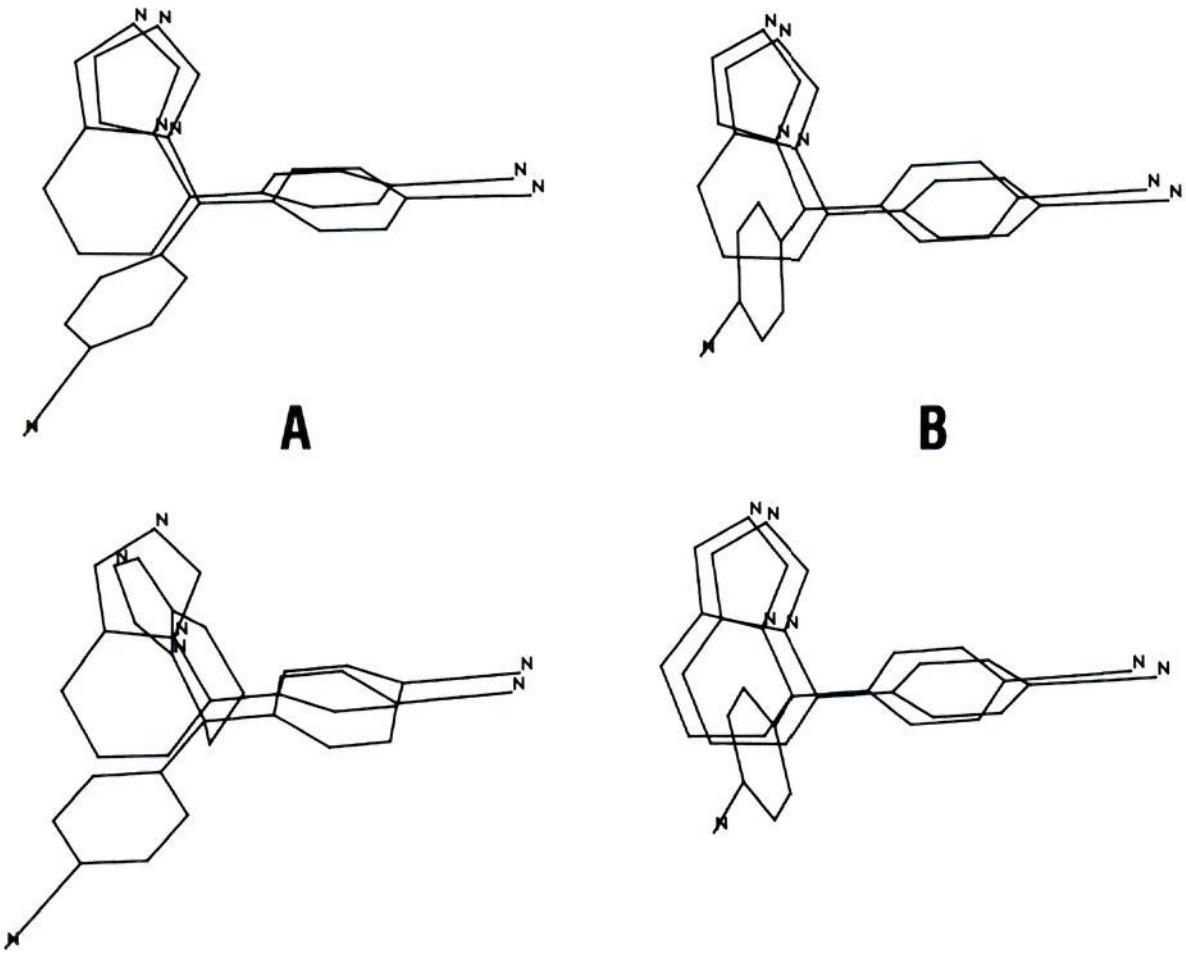

Figure 5. (Top) Two possible modes A and B of superposition of **9** and **4**. (Bottom) **10** can conform to mode B of superposition (right) but does not possess a conformation allowing a good match with the imidazole and cyanobenzyl moieties of **4** according to mode A (left).

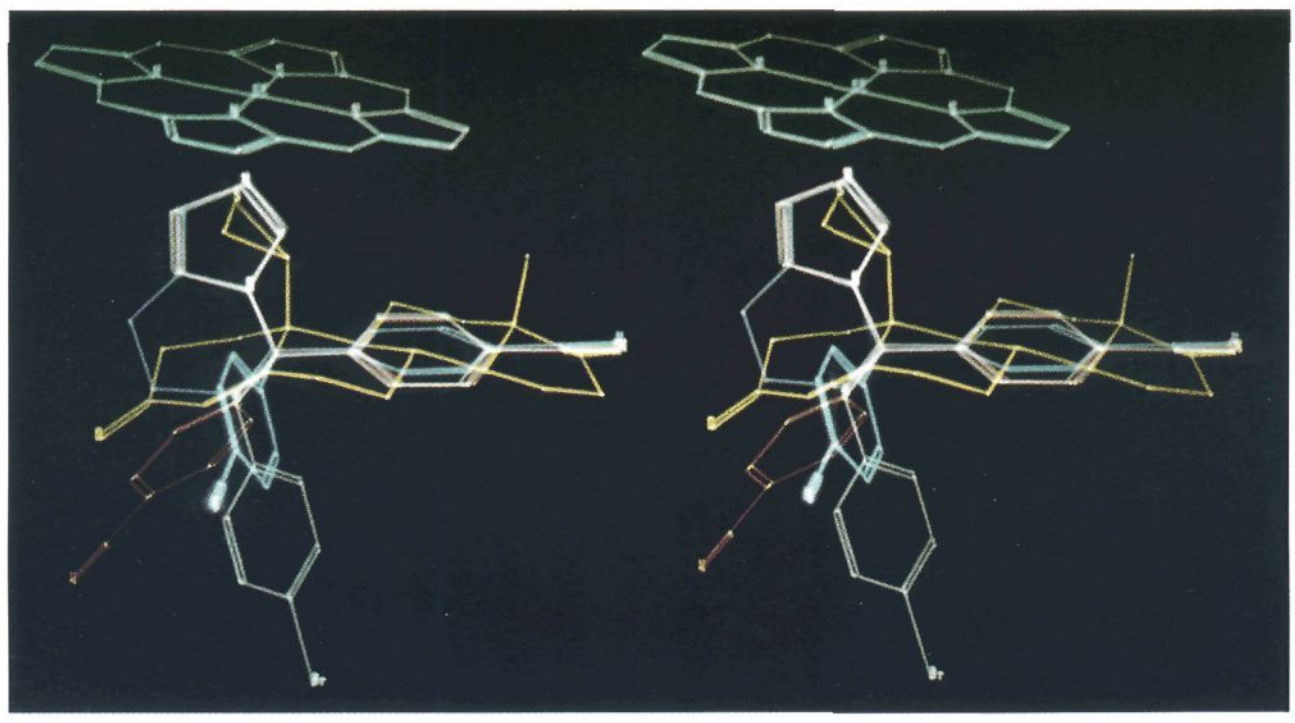

Figure 6. Model of the relative binding modes of **9** (red), **10** (blue), **11** (green), and **7** (yellow) in aromatase's cavity (stereoscopic view).

which one of these two possibilities fits best by considering derivative **10**, a much weaker analogue of **9** (Table I). As shown in Figure 5, while this molecule can conform to mode B of superposition, the conformational restriction caused by the cyclization prevents it from being able to adopt a conformation of type A. Since **10** is significantly less active than its parent molecule, it could be concluded that the mode A of superposition which places the second cyanophenyl ring of **9** on the same side as the α-face of the steroid molecule in the model (Figure 6), precisely in the region located below (with the chosen orientation) the steroid's A ring, is the correct one. Thus, this analysis suggests that there is some room available in the active site of aromatase in the region corresponding to the α-face of the A ring of the steroid ligand whereas the region extending in a perpendicular direction to the long axis of the steroid backbone, which corresponds to the position of the second cyanophenyl moiety of **10** (mode B of superposition) in Figure 6, is not accessible. Whether this is due to the steric reasons or an unfavorable electrostatic effect of the cyano substituent remains to be determined. Another bulky analogue of **3**, compound **11**, has been included in Figure 6. The bromophenyl moiety of this potent aromatase inhibitor (Table I) defines according to our model an additional sterically allowed region of the active site of the enzyme located here below the B ring of the steroid molecule.

Positioning of Other Steroidal Inhibitors. Potent steroidal inhibitors of aromatase derived from AD (**1**) by addition of bulky substituents at certain positions of the molecule have been reported in the literature.[1,2] To gain further insight regarding the volume accessible to ligands in the cavity of the enzyme, representative members of this class of inhibitors have been incorporated in our model. These are 7α-[(4-aminophenyl)thio]androst-4-ene-3,17-dione (7α-APTAD, **12**) (K_i = 18 nM[21]), 7-benzylandrosta-

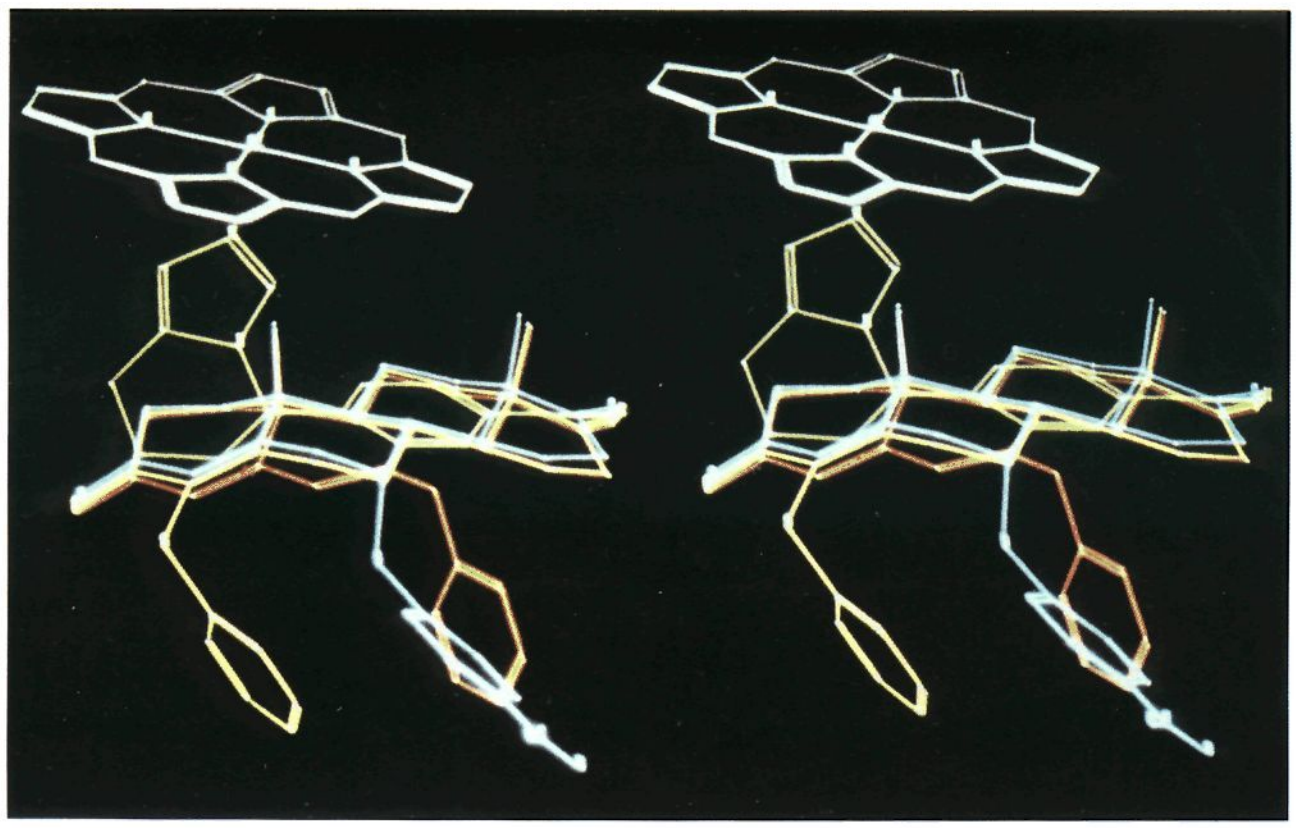

Figure 7. 7a-APTAD (**12**) (blue), 7-BADD (**13**) (red), and 4-PTAD (**14**) (yellow) superimposed on **4** (green) according to the scheme of Figure 3 (stereoscopic view).

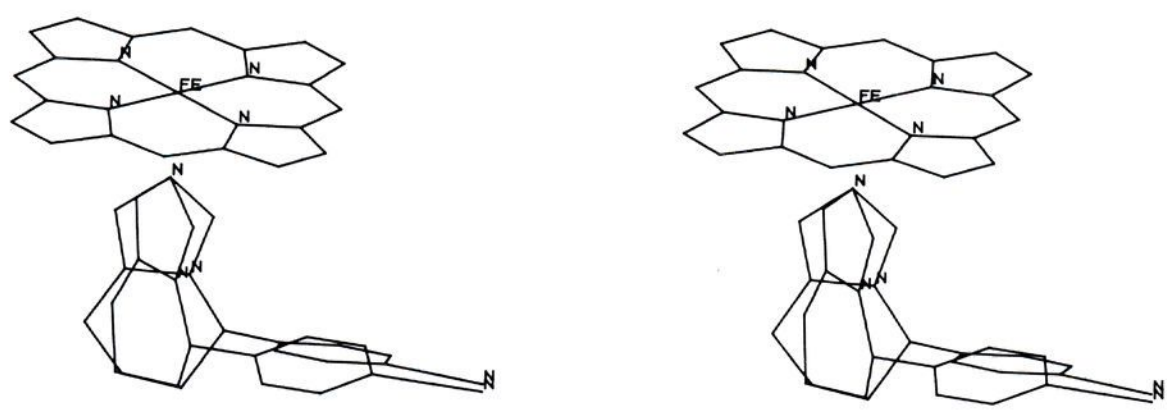

Figure 8. Best fit of the two enantiomers of **3** in terms of cyanophenyl and imidazole moieties overlap. The imidazole ring of the active enantiomer **4** eclipses porphinato Fe–N bonds while that of the inactive enantiomer **5** presents a staggered orientation with respect to the same bonds (stereoscopic view).

4,6-diene-3,17-dione (7-BADD, **13**) (K_i = 61 nM[22]) and 4-(phenylthio)androst-4-ene-3,17-dione (4-PTAD, **14**) (K_i = 34 nM[23]). Figure 7 shows how we position these

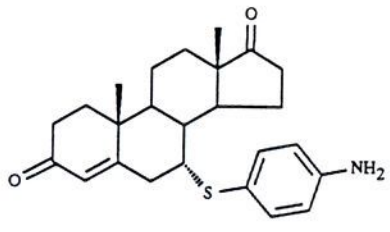

12: 7α-APTAD

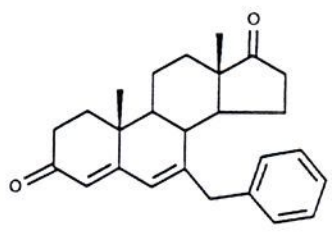

13: 7-BADD

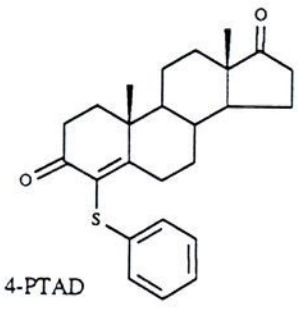

14: 4-PTAD

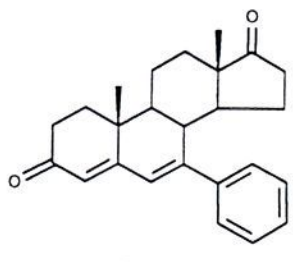

15: 7-PADD

molecules relative to **4**. To obtain this superposition it was assumed that the steroid backbone of these inhibitors could be exactly superimposed on that of 10-thiiranyl-AD (**7**) in the overlay of Figure 3. Although the actual geometry of binding of these inhibitors to aromatase is not directly known, it is unlikely that the active site of the enzyme is versatile enough to strongly bind close structural analogues of its natural substrate in a drastically different geometry. As far as the (aminophenyl)thio and benzyl moieties of 7α-APTAD (**12**) and 7-BADD (**13**) are concerned, their positions in the model were determined by comparing the low-energy conformers of the two molecules and selecting those giving the best overlap of their respective aminophenyl and phenyl rings. As can be seen in Figure 7, a reasonable fit could be obtained in agreement with the results of a modeling study concerning the same compounds recently reported by Li et al.[24] The superposition of these two bulky moieties defines with limited uncertainty the location of a pocket in the active site of aromatase near the 7α-position of the steroid substrate. However, the precise position relatively to the steroid nucleus of the thiophenyl moiety of the 4-substituted analogue **14** in its binding conformation is more uncertain. There are no compounds available allowing a comparison that could remove this conformational uncertainty. In the model of Figure 7, we have chosen to represent this inhibitor in its low-energy conformation that brings its thiophenyl group in the closest proximity with the substituents defining the 7α pocket discussed above.

Explanation for the Low Activity of Compound 5. **5**, the *R*-(+)-enantiomer of fadrozole hydrochloride (**3**), binds to aromatase with an affinity that is 2 orders of magnitude lower than that of the *S*-(−)-enantiomer **4**. To

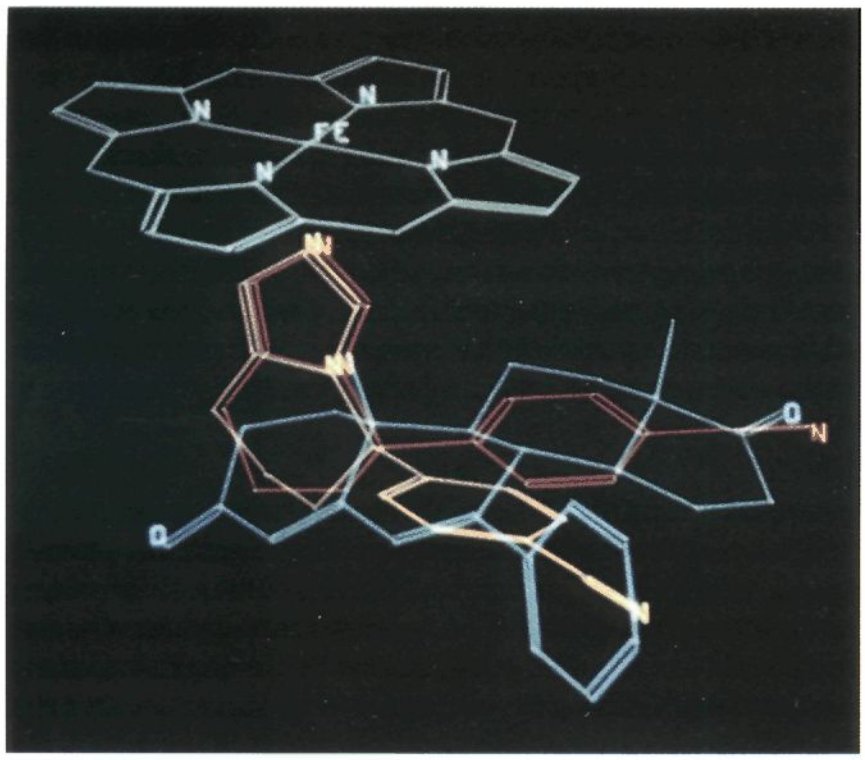

Figure 9. Overlay of **4** (red) and **5** (yellow) obtained by superimposing exactly their respective imidazole rings. The backbone of the steroid derviative 7-PADD (**15**) included in the figure was superimposed on **4** according to the scheme of Figure 3.

explain this stereoselective behavior the following two comparisons of the enantiomers of **3** were made. The overlay of Figure 8 was obtained through superposition of the two molecules by trying to match the positions of their cyanophenyl moieties and heme-coordinating nitrogen atoms of the imidazoles. This figure clearly shows that a good fit of these pharmacophore elements can be achieved. However, in this superposition the planes of the imidazole rings present a dihedral angle of approximately 40°. It has been observed and rationalized in terms of an electronic effect[10] that in metalloporphyrins axial imidazole ligands tend to prefer orientations that eclipse Fe–N bonds of the porphyrin nucleus. In Figure 8 the imidazole ring of the active enantiomer **4** is represented in this orientation which implies an unfavorable staggered orientation for the imidazole ring of the other enantiomer with respect to these Fe–N bonds. An alternative way of superimposing the enantiomers, shown in Figure 9, consists of giving both imidazole rings the favorable eclipsed orientation, i.e. to superimpose them exactly. In such a scheme, the respective cyanophenyl moieties of the two enantiomers point in different directions, and consequently **5**, unlike **4**, is unable to mimic the carbonyl function of the D ring of the steroidal inhibitors. In fact, if the steroid derivative 7-phenylandrosta-4,6-diene-3,17-dione (7-PADD, **15**), a molecule reported to have considerably less affinity for aromatase[22] than its benzyl analogue **13** discussed previously, is included in the superposition as done in Figure 9, it can be seen that its phenyl moiety occupies the same region of space as the cyano group of **5**. This observation suggests the existence of a sterically forbidden area corresponding to this region in the active site of aromatase and offers an explanation for the poor activity of **5**.

Conclusion

In summary, all the molecules discussed have been superposed together (Figure 10) and the accessible and nonaccessible volumes to ligands displayed. The resulting picture suggests that aromatase's cavity is quite large with a pocket available in the region located below the α-face of the steroidal substrates, distal to the heme group of the enzyme. In contrast, the wall of the cavity seems to lie close to the edge of the steroid ligands corresponding to the 4-, 5-, 6- and 7-positions of their backbones from which substituents of the almost inactive ligands **5**, **10**, and **15** protrude. Our studies give strong support to the hypothesis that the cyanobenzyl moiety present in the imidazole-type inhibitors partially mimic the steroid backbone of the enzyme's natural substrate AD (**1**) as previously proposed by Banting et al.[19] and more recently by Van Roey et al.[25] However, in contrast to these authors we propose that it is not the A ring of the steroidal substrates which is mimicked by the azole-type inhibitors but rather structural features belonging to rings C and D.

Work is in progress to include the third important class of aromatase inhibitors, the analogues of aminoglutethimide, in this model which is currently being used in the design of new types of inhibitors.

Experimental Section

Molecular Modeling. Conformational Analyses. Each compound discussed in this study was subjected to a systematic conformational analysis to derive all its minimum-energy conformations. The starting conformations were generated by the CONCEPTOR program[26] and subsequently energy minimized in BATCHMIN[27] using the NCC force field.[28] Only the minimized conformations whose relative energy with respect to the global minimum did not exceed 3 kcal/mol were retained in the superposition studies.

Superpositions. The superpositions were performed in the GRASP program.[29] This program can handle molecules as ensembles of conformations and is mainly used to determine the

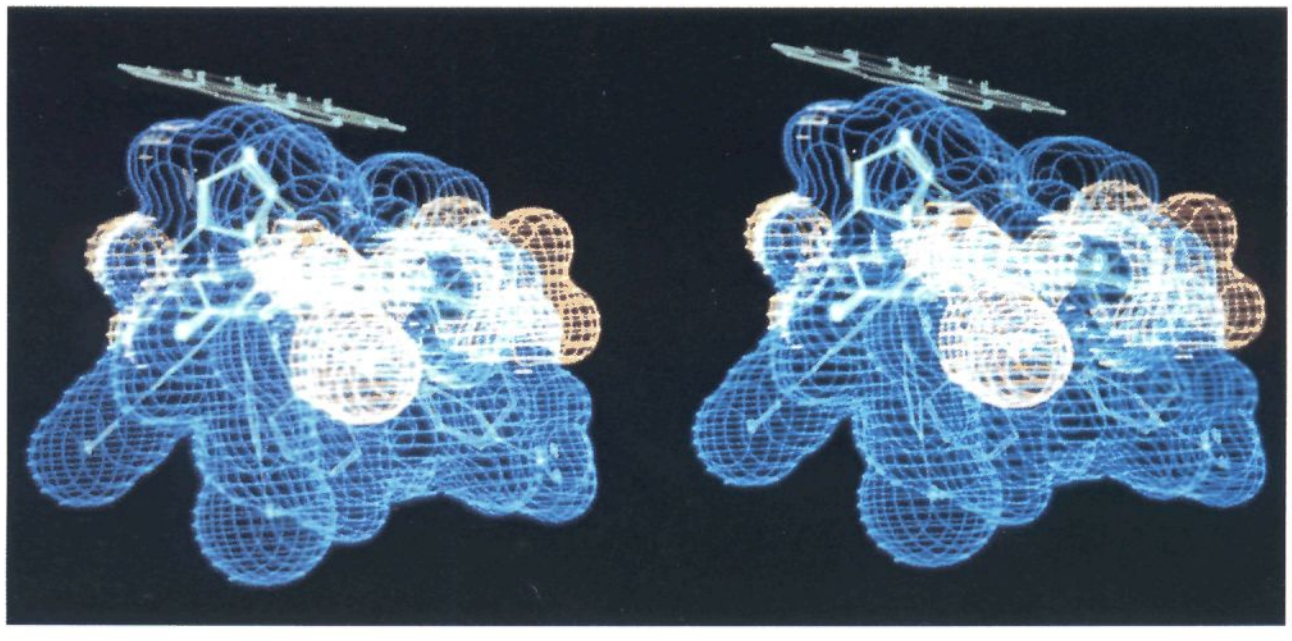

Figure 10. Stereoscopic view of the accessible (blue) and nonaccessible (red) volumes to ligands in the active site of aromatase.

conformation of a molecule that gives the best fit to a template structure according to a given superposition scheme. The pictures showing the superpositions were produced in MACROMODEL Version 2.0.[30]

Molecular Volumes. The accessible and nonaccessible volumes to ligands shown in Figure 10 are defined respectively as the sum of the molecular volumes of the highly active inhibitors and as the volume that the weakly active inhibitors do not share with this accessible volume. They were calculated and displayed using the method of Bohacek et al.[31] incorporated in MACROMODEL Version 2.0.

Single-crystal X-ray analysis: $(C_{14}H_{14}N_3)^+(C_4H_5O_6)^-$, FW = 373.37, colorless, monoclinic, space group $P2_1$, a = 7.620(1) Å, b = 8.280(1) Å, c = 14.653(1) Å, β = 94.89(1)°, V = 921.1(3) Å^3, z = 2, D_{calc} = 1.345 g/cm^3, μ_{Cu} = 8.2 cm^{-1}. The cell constants were determined from a least-squares fit of the setting angles for 25 accurately centered reflections. An Enraf-Nonius CAD4 automatic diffractometer was used for data collection using graphite-monochromated Cu Kα radiation and ω-2θ scan technique. The intensities of 2200 independent reflections with $\theta < 75°$ were measured, of which 1974 were classified as observed with $I > 3\sigma(I)$. Raw intensities were reduced to structure factor amplitudes by correction for scan speed, background, and Lorentz and polarization effects. Absorption corrections were not applied.

The structure was solved by direct methods (SDP MULTAN 82). All hydrogen atoms were located on a difference Fourier map. The structure was refined by full-matrix least-squares calculations with anisotropic (isotropic for hydrogen atoms) thermal parameters to a final R value of 0.085. The absolute configuration of 4 was given by D-(−)-tartaric acid (Figure 1).

Biology. Inhibition of Human Placental Aromatase in Vitro. The microsomal fraction of fresh human term placenta was obtained using the method described by Thompson and Siiteri.[32] The assay procedure for the determination of IC_{50} values was carried out as described previously.[33] Briefly, incubations contained [4-^{14}C]androstenedione (240 nM), excess NADPH (240 μM), microsomal protein (50 μg), and varying concentrations of inhibitor in phosphate buffer (0.05 M, pH 7.4) in a final volume of 1 mL. The incubation was carried out at 37 °C. The reaction was started by the addition of enzyme and stopped after 20 min by the addition of diethyl ether (7 mL). Following extraction and centrifugation, the organic layer was removed, evaporated to dryness, taken up in acetone, and chromatographed on silica gel 60 thin-layer plates using $CHCl_3$/MeOH (95/5 by volume). Radioactivity was measured on a Berthold TLC digital autoradiograph linked to a COMPAQ 386/20 computer. Spots corresponding to estrone, estradiol, and androstenedione were integrated. The IC_{50} was determined by plotting the reciprocal of the percent conversion versus the inhibitor concentration in a Dixon plot.[34]

Chemistry. Melting points were determined on a Reichert Thermovar and are uncorrected. ^{1}H-NMR spectra were recorded on a Varian Gemini 200 or Bruker Spectrospin HX-360 spectrometer with TMS as internal standard. Chemical shifts are given in ppm relative to TMS as internal standard. Fast atom bombardment mass spectra (FAB-MS) were recorded with a ZAB HF spectrometer (Fisons Instruments). For column chromatography, silica gel 60 (Merck) was used. Elemental analyses were within 0.4% of the theoretical value. The HPLC experiments were performed with a modular liquid chromatograph compared of a Shimadzu LC-6A pump and a multiwavelength Shimdazu UV–vis detector Model SPD-6AV in series with a Perkin-Elmer polarimeter (Model 241 LC) equipped with a 80-μL cell (length 10 cm). Both signals (UV absorption and optical rotation) were recorded and processed by an IBM PC-AT3 microcomputer, via a Dysc WD 24 analog interface module using the Maxima 820 chromatographic software (Carlo Erba, Milan, Italy). For preparative resolutions a Shimadzu LC-8A pump has been used, and the polarimeter has been equipped with a 1-mL flow cell.

Separation of the Enantiomers 4 and 5 of (+)-Fadrozole Hydrochloride (3) by HPLC. The analytical and preparative chromatographic separations of the enantiomers of 3 have been performed on benzoylcellulose beads as a stationary phase, using the columns described elsewhere.[5] The separation factor on the analytical column was 3.55 with 6:4 hexane/2-propanol as a mobile phase, and the (−)-enantiomer 4 eluted first. For analytical determinations of the optical purity, a Chiralcel OD column (Daicel Chemical Industries, Tokyo, Japan) has also been used, but the elution order is inverted (separation factor α = 1.40 with 7:3 hexane/2-propanol as a mobile phase). About 3 g of the racemate 3 was repetitively resolved on the preparative column (75 cm × 5-cm i.d.), using 65:35 hexane/2-propanol as a mobile phase at a flow rate of 50 mL/min. The first-eluted (−)-enantiomer 4 (21.3 g obtained in 50 runs) was dissolved in 35 °C in EtOAc and treated for 20 min with 1 g of charcoal to give after filtration and evaporation 20.3 g of pure 4 as white crystals. 4 (20.1 g, 90.1 mmol) was then dissolved in acetone (450 mL) and treated with an 0.73 N ethereal HCl solution (186 mL, 135 mmol) for 15 min to give after evaporation and crystallization from diethyl ether 23 g (88.6 mmol, 98%) of the hydrochloride of 4 as hygroscopic crystals of mp 218.5 °C: $[\alpha]^{20}_D$ (c 0.53, EtOH) −95.3 ± 1.9°; MS (FAB) m/e 224 (M + H$^+$). A 5.6-g (25.1-mmol) sample of the second eluted (+)-enantiomer 5 was dissolved in n-BuOH/H_2O, 9:1 (75 mL), at 60–70 °C and treated with 75 mL of a warm solution of (−)-bis-*O*,*O*′-(4-toluoyl)tartaric acid (11.4 g, 28.2 mmol) in n-BuOH/H_2O (9:1). The crystalline diastereomeric salt was filtered off, washed with diethyl ether, and afforded after treatment with aqueous $NaHCO_3$ and a standard workup procedure 5.4 g (24.18 mmol, 96%) of 5. This material was converted in analogy to the above described procedure in the **hydrochloride of 5** (6.2 g, 23.9 mmol; 98.8%): mp 213.4 °C; $[\alpha]^{20}_D$ (c 0.495, EtOH) +94.3 ± 2.0°; MS (FAB) m/e 224 (M + H$^+$).

Tartrate of 4. A solution of 4 (112 mg, 0.5 mmol) in absolute ethanol (5 mL) is treated by a solution of D-(−)-tartaric acid (75 mg, 0.5 mmol) in ethanol (5 mL). The reaction mixture was evaporated to an oily residue which crystallized from diethyl ether to yield 150 mg (0.4 mmol, 80%) of the **tartrate of 4**: mp 155–157 °C; $[\alpha]^{20}_D$ (c 0.587, EtOH) −79.7 ± 1.7°. An additional recrystallization from ethanol gave the **tartrate of 4** as colorless needles adequate for X-ray crystallography.

1-(1-Imidazolyl)-3,4-tetrahydro-6-cyanotetralin (8). To a well-stirred solution of imidazole (272 mg, 4 mmol) in CH_2Cl_2 (2.5 mL) was added thionyl chloride (0.175 mL, 2.4 mmol). The white suspension was reacted in portions with 6-cyano-1-tetralone[7] (342 mg, 2 mmol) and stirred at room temperature for 3 h and an additional 7 h at 40 °C. The reaction mixture was then treated by a solution of K_2CO_3 (386 mg, 2.8 mmol) in 1.6 mL of H_2O and extracted with $CHCl_3$. The combined extracts were dried over anhydrous sodium sulfate and evaporated. The residue was chromatographed on silica gel [elution with hexane/ethyl acetate (1:2)] to yield 50 mg (0.23 mmol, 11.2%) of product 8 as a colorless solid: mp 152–153 °C (after crystallization from diethyl ether); ^{1}H NMR (360 MHz, $CDCl_3$) δ 7.58 (1 H, dd, J = 1.6, 0.8 Hz), 7.47 (1 H, d, J = 8.2 Hz), 7.43 (1 H, dd, J = 8.2, 1.9 Hz), 7.19 (1 H, dd, J = 1.6, 0.8 Hz), 6.99 (1 H, dd, J = 1.6, 1.6 Hz), 6.81 (1 H, d, J = 8.2 Hz), 6.28 (1 H, t, J = 4.8 Hz), 2.93 (2 H, t, J = 8.23 Hz), 2.55 (2 H, dt, J = 8.23, 4.8 Hz). Anal. ($C_{14}H_{11}N_3$) C: calcd, 76.00; found, 75.55; H, N.

5,5-Bis(4-cyanophenyl)-5,6,7,8-tetrahydroimidazo[1,5-*a*]pyridine (10). To a stirred mixture of potassium *tert*-butylate (617 mg, 5.5 mmol) in absolute DMF (3 mL) was added over 30 min a solution of free base of 3 (445.4 mg, 2 mmol) in absolute DMF (3 mL). The reaction mixture was stirred at room temperature for 30 min, and while the temperature was maintained at 20 °C, treated by dropwise addition of a solution of 4-fluorobenzonitrile (303 mg, 2.5 mmol) in absolute DMF (3 mL). After an additional stirring for 1.5 h at room temperature, the reaction mixture was cooled to 0 °C, diluted with CH_2Cl_2, and neutralized with 6 N HCl to pH 7.3. During this addition the temperature was kept at −5 °C. Evaporation of the solvent, partitioning of the residue between H_2O and CH_2Cl_2, washing of the organic phase with brine, drying over sodium sulfate, and evaporation gave the crude product. The latter was chromatographed on silica gel with $CHCl_3$ to yield **10** (317 mg, 49%): mp 185–186 °C (after crystallization from CH_2Cl_2/Et_2O); ^{1}H NMR (360 MHz, $CDCl_3$) δ 7.65 (4 H, dd, J = 8.4, 2.0 Hz), 7.1 (4 H, dd, J = 8.4, 2.0 Hz), 6.92 (1 H, m), 6.90 (1 H, d, J = 1.0 Hz), 2.91 (2 H, m), 2.66 (2 H, m), 1.61 (2 H, m); MS (FAB) m/e 325 (M + H$^+$). Anal. ($C_{21}H_{16}N_4$) C, H, N.

1-[(4-Cyanophenyl)-1-[(4-bromophenyl)imino]methyl]-1*H*-imidazole (11). A well-stirred solution of 4-bromoaniline (1 g, 5.5 mmol) in pyridine (24 mL) was treated in portions with 4-cyanobenzoyl chloride (820 mg, 5 mmol) and heated to 45 °C for 1 h. The reaction mixture was cooled to 0 °C and poured into 200 mL of an ice-cooled 2 N HCl solution. After the mixture was stirred for 15 min the crude *N*-(4-bromophenyl)-4-cyanobenzamide was filtered off, washed four times with water, and dried under reduced pressure. This material (252 mg, 0.837 mmol) was dissolved in C_6H_6 (1.6 mL) and treated with PCl_5 (191 mg, 0.92 mmol). The reaction mixture was stirred at 80 °C and after the end of HCl evolution for an additional 2 h at room temperature. After evaporation to dryness the crude imidoyl chloride was dissolved in glyme (1.6 mL) and added dropwise to a cooled solution of imidazole (171 mg, 2.5 mmol) in glyme (0.8 mL). The reaction mixture was stirred overnight at room temperature, diluted with H_2O, and extracted with diethyl ether. The extracts were combined, dried (anhydrous sodium sulfate), and concentrated. The yellow solid was chromatographed on silica gel [elution with hexane/EtOAc (2/1)] to yield 11 (225 mg, 69.5%) as a colorless solid: mp 153–156 °C (after crystallization from diethyl ether); ^1H NMR (360 MHz, $CDCl_3$) δ 7.78 (1 H, dd, J = 1.5, 0.8 Hz), 7.68 (2 H, m), 7.43 (1 H, dd, J = 1.5, 1.5 Hz), 7.37 (2 H, m), 7.28 (2 H, m), 7.15 (1 H, dd, J = 1.5, 0.8 Hz), 6.55 (2 H, m). Anal. ($C_{17}H_{11}N_4Br$) H, N, Br.

Supplementary Material Available: Elemental analytical data for new compounds and X-ray data (5 pages). Ordering information is given on any current masthead page.

Acknowledgment. We thank W. Beck, D. Folio, M. Frey, S. Maggio, and I. Pieragostino for their skillful experimental work, P. Richert for performing chromatographical resolutions, and S. Moss and Dr. H. Fuhrer for their significant spectroscopic contribution.

References

(1) Cole, P. A.; Robinson, C. H. Mechanism and Inhibition of Cytochrome P-450 Aromatase. *J. Med. Chem.* **1990**, *33*, 2933–2942.
(2) Banting, L.; Nicholls, P. J.; Shaw, M. A.; Smith, H. J. Recent Developments in Aromatase Inhibition as a Potential Treatment for Estrogen-Dependent Breast Cancer. In *Progress in Medicinal Chemistry, V.26*; Ellis, G. P., West, G. B., Eds.; Elsevier Science Publishers, B. V.: Amsterdam, 1989; pp 253–298.
(3) Van Wauwe, J. P.; Janssen, P. A. J. Is There a Case for P-450 Inhibitors in Cancer Treatment? *J. Med. Chem.* **1989**, *32*, 2232–2239.
(4) Browne, L. J.; Gude, C.; Rodriguez, H.; Steele, R. E.; Bhatnagar, A. S. Fadrozole Hydrochloride: A Potent, Selective, Nonsteroidal Inhibitor of Aromatase for the Treatment of Estrogen-Dependent Disease. *J. Med. Chem.* **1991**, *34*, 725–736.
(5) Francotte, E.; Wolf, R. M. Benzoyl Cellulose Beads in the Pure Polymeric Form as a New Powerful Sorbent for the Chromatographic Resolution of Racemates. *Chirality* **1991**, *3*, 43–55.
(6) Bowman, R. M.; Steele, R. E.; Browne, L. J. U.S. Patent 4,937,250, 1990.
(7) Itoh, K.; Miyake, A.; Tada, N.; Hirata, M.; Oka, Y. Synthesis and b-Adrenergic Blocking Activity of 2-(N-Substituted amino)-1,2,3,4-tetrahydronaphtalen-1-ol Derivatives. *Chem. Pharm. Bull.* **1984**, *32*, 130–151.
(8) Ugi, I.; Beck, F.; Fetzer, U. Hydrolyse von Carbonsäureimidchloriden. *Chem. Ber.* **1962**, *95*, 126–135.
(9) Kellis, T. J.; Childers, W. E.; Robinson, C. H.; Vickery, L. E. Inhibition of Aromatase Cytochrome P-450 by 10-Oxirane and 10-Thiirane Substituted Androgens. *J. Biol. Chem.* **1987**, *262*, 4421–4426.
(10) Sheidt, W. R.; Chipman, D. M. Preferred Orientation of Imidazole Ligands in Metalloporphyrins. *J. Am. Chem. Soc.* **1986**, *108*, 1163–1167.
(11) Mashiko, T.; Reed, C. A.; Haller, K. J.; Kastner, M. E.; Scheidt, W. R. Thioether Ligation in Iron-Porphyrin Complexes: Models for Cytochrome c. *J. Am. Chem. Soc.* **1981**, *103*, 5758–5767.
(12) Rosenfield, R. E.; Parthasarathy, R.; Dunitz, J. D. Directional Preferences for Non-Bonded Atomic Contacts with Divalent Sulfur. 1. Electrophiles and Nucleophiles. *J. Am. Chem. Soc.* **1977**, *99*, 4860–4862.
(13) Chakrabarti, P. Geometry of Interaction of Metal Ions with Sulfur-Containing Ligands in Protein Structures. *Biochemistry* **1989**, *28*, 6081–6085.
(14) (a) Allen, F. H.; Bellard, S.; Brice, M. D.; Cartwright, B. A.; Doubleday, A.; Higgs, H.; Hummelink, T.; Hummelink-Peters, B. G.; Kennar, O.; Motherwell, W. D. S.; Rodgers, J. R.; Watson, D. G. The Cambridge Crystallographic Database. *Acta Crystallogr.* **1979**, *B39*, 2331. (b) Scheidt, W. R.; Oswath, S. R.; Lee, Y. J. Crystal and Molecular Structure of Bis-imidazole-(meso-tetraphenylporphynato)-iron-(III)-chloride. A Classic Molecule Revisited. *J. Am. Chem. Soc.* **1987**, *109*, 1958–1963.
(15) Unpublished results.
(16) Numazawa, M.; Mutsumi, A. 6-alpha, 7-alpha-Cyclopropane Derivatives of Androstene-4-ene: a Novel Class of Competitive Aromatase Inhibitors. *Biochem. Biophys. Res. Commun.* **1991**, *177*, 401–406 and references therein.
(17) Numazawa, M.; Mutsumi, A.; Hoshi, K.; Oshibe, M.; Ishikawa, E.; Kigawa, H. Synthesis and Biochemical Studies of 16- and 19-Substituted Androstene-4-enes as Aromatase Inhibitors. *J. Med. Chem.* **1991**, *34*, 2496–2504.
(18) Sherwin, P. F.; McMullan, P. C.; Covey, D. F. Effects of Steroid D-ring Modification on Suicide Inactivation and Competitive Inhibition of Aromatase by Analogues of Androsta-1,4-diene. *J. Med. Chem.* **1989**, *32*, 651–658.
(19) Banting, L.; Smith, H. J.; James, M.; Jones, G.; Nazareth, W.; Nicholls, P. J.; Hewlins, M. J. E.; Rowlands, M. G. Structure-Activity Relationships for Non-Steroidal Inhibitors of Aromatase. *J. Enzyme Inhib.* **1988**, *2*, 215–229.
(20) Bullion, K. A.; Osawa, Y.; Braun, D. G. Reversible Inhibition of Human Placental Microsomal Aromatase by CGS 18320B and other Non-Steroidal Compounds. *Endocrine Res.* **1990**, *16*, 255–267.
(21) Brueggemeier, R. W.; Floyd, E. E.; Counsell, R. E. Synthesis and Biochemical Evaluation of Inhibitors of Estrogen Biosynthesis. *J. Med. Chem.* **1978**, *21*, 1007–1011.
(22) Li, P. K.; Brueggemeier, R. W. Synthesis and Biochemical Studies of 7-Substituted-androsta-4,6-diene-3,17-diones as Aromatase Inhibitors. *J. Med. Chem.* **1990**, *33*, 101–105.
(23) Abul-Hajj, Y. J. Aromatase Inhibition by 4-Thiosubstitutedandrost-4-ene-3,17-dione Derivatives. *J. Steroid Biochem.* **1990**, *35*, 139–143.
(24) Li, P. K.; Brueggemeier, R. W. 7-Substituted Steroidal Aromatase Inhibitors: Structure-Activity Relationships and Molecular Modeling. *J. Enzyme Inhib.* **1990**, *4*, 113–120.
(25) Van Roey, P.; Bullion, K. A.; Osawa, Y.; Browne, L. J.; Bowman, R. M.; Braun, D. G. Structure-Activity Studies of Non-Steroidal Aromatase Inhibitors: the Crystal and Molecular Structures of CGS 16949A and CGS 18320B. *J. Enzyme Inhib.* **1991**, *5*, 119–132.
(26) CONCEPTOR: in house molecular modeling program written by Cohen, N. C.; similar to SCRIPT: Cohen, N. C.; Colin, P.; Lemoine, G. *Tetrahedron* **1981**, *37*, 1711.
(27) Still, W. C.; Mohamadi, F.; Richards, N. G. J.; Guida, W. C.; Liskamp, R.; Lipton, M.; Caufield, C.; Hendrickson, T. *BATCHMIN V2.0*; Department of Chemistry, Columbia University: New York.
(28) For the NCC force field, see: Cohen, N. C. In *Advances in Drug Research*; Testa, B., Ed.; Academic Press: New York, 1985; Vol. 14, p 50 and references therein.
(29) GRASP: "Graphics Applied to the Superpositioning Problem"; in-house molecular modeling program written by Pearson, J. E. A short description of the program is given in Bühlmayer, P.; Criscione, L.; Fuhrer, W.; Furet, P.; De Gasparo, M.; Stutz, S.; Whitebread, S. *J. Med. Chem.* **1991**, *34*, 3105–3114.
(30) Still, W. C.; Mohamadi, F.; Richards, N. G. J.; Guida, W. C.; Liskamp, R.; Lipton, M.; Caufield, C.; Hendrickson, T. *MACROMODEL V2.0*; Department of Chemistry, Columbia University: New York.
(31) Bohacek, R. S.; Guida, W. C. A Rapid Method for the Computation, Comparison and Display of Molecular Volumes. *J. Mol. Graph.* **1989**, *7*, 113–117.
(32) Thompson, E. A.; Siiteri, P. K. Utilization of Oxygen and Reduced Nicotinamide Adenine Dinucleotide Phosphate by Human Placental Microsomes during Aromatization of Androstenedione. *J. Biol. Chem.* **1974**, *249*, 5364–5372.
(33) Purba, H. S.; Bhatnagar, A. S. A Comparison of Methods measuring Aromatase Activity in Human Placenta and Rat Ovary. *J. Enzyme Inhib.* **1990**, *4*, 169–178.
(34) Cheng, J.-C.; Prusoff, W. H. Relationship between the Inhibition Constant (K_i) and the Concentration of Inhibitor which causes 50% Inhibition (IC50) of an Enzymatic Reaction. *Biochem. Pharmacol.* **1973**, *22*, 3099–3108.